Original Article

JCBFM

Journal of Cerebral Blood Flow & Metabolism
2021, Vol. 41(8) 1842–1857

DOI: 10.1177/0271678X20980296
journals.sagepub.com/home/jcbfm
SAGE

Role of perivascular and meningeal macrophages in outcome following experimental subarachnoid hemorrhage

Hoyee Wan[1,2,3], Shakira Brathwaite[1,3], Jinglu Ai[1,4], Kullervo Hynynen[2,3] and R Loch Macdonald[1,5]

Abstract

The distribution and clearance of erythrocytes after subarachnoid hemorrhage (SAH) is poorly understood. We aimed to characterize the distribution of erythrocytes after SAH and the cells involved in their clearance. To visualize erythrocyte distribution, we injected fluorescently-labelled erythrocytes into the prechiasmatic cistern of mice. 10 minutes after injection, we found labelled erythrocytes in the subarachnoid space and ventricular system, and also in the perivascular spaces surrounding large penetrating arterioles. 2 and 5 days after SAH, fluorescence was confined within leptomeningeal and perivascular cells. We identified the perivascular cells as perivascular macrophages based on their morphology, location, Iba-1 immunoreactivity and preferential uptake of FITC-dextran. We subsequently depleted meningeal and perivascular macrophages 2 days before or 3 hours after SAH with clodronate liposomes. At day 5 after SAH, we found increased blood deposition in mice treated prior to SAH, but not those treated after. Treatment post-SAH improved neurological scoring, reduced neuronal cell death and perivascular inflammation, whereas pre-treatment only reduced perivascular inflammation. Our data indicate that after SAH, erythrocytes are distributed throughout the subarachnoid space extending into the perivascular spaces of parenchymal arterioles. Furthermore, meningeal and perivascular macrophages are involved in erythrocyte uptake and play an important role in outcome after SAH.

Keywords

Perivascular macrophage, subarachnoid hemorrhage, clodronate liposome, erythrocytes, inflammation

Received 13 June 2020; Revised 12 November 2020; Accepted 14 November 2020

Introduction

Subarachnoid hemorrhage (SAH) is a subtype of stroke most commonly caused by the rupture of an intracranial aneurysm. Although it only comprises 7% of all strokes, the early age of onset and high morbidity result in SAH contributing disproportionately to the number of life years lost to stroke.[1,2] Key processes contributing to morbidity after SAH include early brain injury and delayed cerebral ischemia (DCI).[3,4] Early brain injury occurs minutes to hours after SAH and is due to subarachnoid blood, and in some cases, the increase in intracranial pressure. DCI occurs in 30% of SAH patients 4–14 days after the ictus.[5] The mechanisms underlying DCI are multi-factorial and are partially attributed to the degeneration of erythrocytes that are trapped in the subarachnoid space.[5] As erythrocytes break down, substances including heme, free iron and bilirubin are produced, which can cause vasoconstriction, inflammation and direct cellular injury.[6–8]

[1]Division of Neurosurgery, St. Michael's Hospital, Toronto, Canada
[2]Department of Medical Biophysics, University of Toronto, Toronto, Canada
[3]Sunnybrook Health Sciences Research Institute, Sunnybrook Hospital, Toronto, Canada
[4]Barrow Neurological Institute, Phoenix, AZ, USA
[5]Department of Neurological Surgery, University of California San Francisco, Fresno, CA, USA

Corresponding author:
R Loch Macdonald, Department of Neurological Surgery, UCSF Fresno, Fresno, CA, USA.
Email: rlochmacdonald@gmail.com

Recent studies have suggested that parenchymal microglia mediate the clearance of erythrocytes and their breakdown products from the subarachnoid space.[9–12] However, it is unclear how microglia can come into contact with erythrocytes, as the blood should be primarily contained within the subarachnoid space surrounding the brain. Blood may potentially enter the perivascular spaces of vessels that penetrate into the brain parenchyma (i.e., Virchow-Robin spaces), which are usually reported to be continuous with the subarachnoid space.[13,14] In both animal models and human studies of SAH, blood is found macroscopically distributed along the surface pial vessels, and blood coagulation products have been detected in the parenchymal perivascular space.[14] In autopsy samples of SAH patients, intact erythrocytes have been found in the perivascular space surrounding large cortical penetrating vessels, though the type of vessel and location relative to the basal blood clot was not characterized.[14] It is currently unclear how far these erythrocytes extend into the parenchymal perivascular space, how they are cleared, or if they contribute to injury after SAH. Confirmation and elaboration of these histological findings using fluorescently-labelled erythrocytes may thereby reveal insight into the distribution of blood after SAH, particularly within parenchymal perivascular spaces. Furthermore, by using a membrane-bound dye, we can visually identify the cells that are directly involved in the clearance of subarachnoid blood. Importantly, erythrocytes were chosen for this study, rather than other blood elements, as they are the most abundant cell type in the blood and are known to contribute to the pathogenesis after SAH.[15]

In the current study, we first investigated the spatial and temporal distribution of erythrocytes after SAH and identified the key cells involved in their clearance as perivascular and meningeal macrophages. We additionally evaluated the role of these macrophages in mediating neurological outcome using a well-established prechiasmatic blood injection model of SAH. These findings provide novel insights into how blood is distributed and cleared, and suggest the importance of perivascular and meningeal macrophages in outcome after SAH.

Methods

Animals

All experimental protocols in this study were approved by the Institutional Animal Care and Use Committee at St. Michael's Hospital and conducted in accordance with the regulations outlined by the Canadian Council on Animal Care and the Animal Research: Reporting of *in Vivo* Experiments (ARRIVE) guidelines. 4-month old male CD1 mice (35–45 g) (Charles River, Quebec, ON) were used in this study, and all were housed in a 12:12 light/dark cycle with controlled humidity and temperature with access to food and water *ad libitum*. Animal experiments were all conducted in the afternoon. 62 mice were randomized into two experimental groups, 1) Labeled blood cell injection: sacrifice at 10 minutes ($n = 5$), 2 days ($n = 5$ for scanning, $n = 5$ for immunofluorescence experiments) and 5 days ($n = 5$ for scanning, $n = 5$ for immunofluorescence experiments, $n = 5$ mice injected with FITC-dextran for perivascular macrophage labelling), 2) Liposome injection (clodronate/PBS liposomes 2 days before SAH, clodronate/PBS liposomes 3 hours after SAH, $n = 6$ per group) (Figure 1(a) and (b)). In addition to these main groups, we included clot burden data from a pilot study ($n = 5$ pre-treated, and $n = 3$ post treated) exploring the feasibility of injecting clodronate and subarachnoid blood considering the increased intracranial volume needed to be injected (see statistical analysis for more information). 41 mice in total were used as donor mice. For erythrocyte tracking experiments, we harvested blood from 9 mice to isolate erythrocytes (enough erythrocytes were isolated from one animal to inject 3–4 mice). For clodronate experiments, whole blood was used, which was obtained from 32 mice.

Red blood cell isolation and labelling

Whole blood was collected by cardiac puncture and mixed with heparin. Erythrocytes were separated from plasma by centrifugation for 10 minutes at 500 x *g* at room temperature. The pellet was washed thoroughly with cell wash buffer (21.0 mM Tris, 4.7 mM KCl, 2.0 mM $CaCl_2$,140.5 mM NaCl, 1.2 mM $MgSO_4$, 5.5 mM glucose and 0.5% Bovine Serum Albumin (BSA), $pH = 7.40$). The pellet was washed again and spun twice. 100 µL of pellet was added to 900 µL of cell wash buffer and 10 µL of Vybrant™ CM-DiI (ThermoFisher Scientific, Waltham, MA). Cells were incubated for 45 minutes on a shaker at 37 °C. Cells were spun down at 250 x *g* and washed three times with cell wash buffer. Cells were imaged to observe cellular purity, viability and integration of dye into cell membrane (Supplemental Figure 1). Cells were prepared, stored at 37 °C and used within 3 hours of labelling. Immediately prior to injection into the subarachnoid space, cells were mixed with artificial CSF (119 mM NaCl, 26.2 mM $NaHCO_3$, 2.5 mM KCl, 1 mM Na_2HPO_4, 1.3 mM $MgCl_2$ and 10 mM glucose, $pH = 7.4$), to maintain a similar volume-to-cell ratio as whole blood.

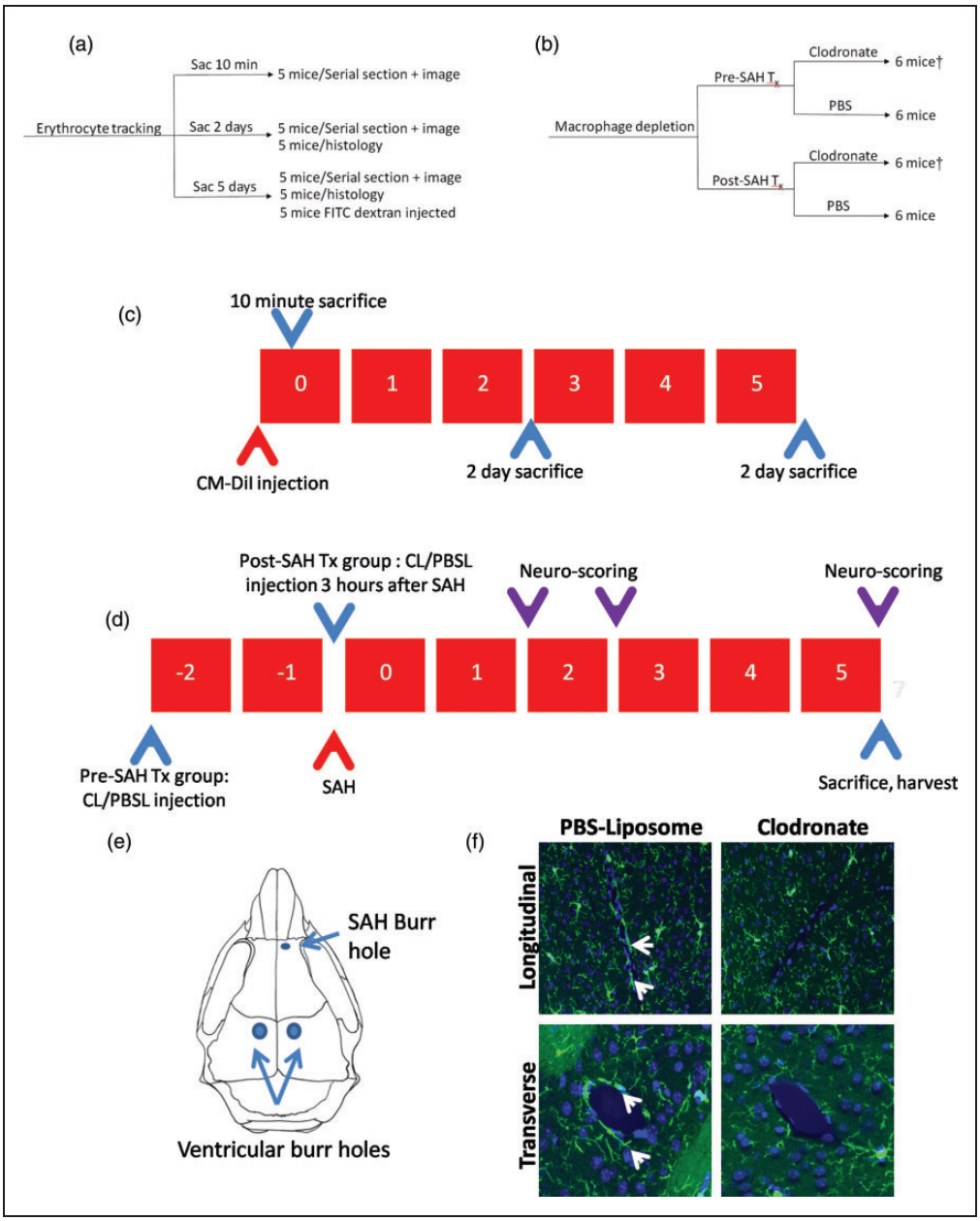

Figure 1. Allocation of mice and experimental design. (a) Allocation of mice in erythrocyte tracking experiments. (b) Allocation of mice in macrophage depletion experiments (Tx=treatment). †indicates a pilot group of mice, that were used only for analysis of clot burden (n = 3 mice for post-SAH clodronate treatment and n = 5 mice for post-SAH clodronate treatment). (c) Sacrifice timeline of mice in the erythrocyte tracking experiments. Mice were sacrificed at 10 minutes, 2 days and 5 days after SAH onset. (d) Design of macrophage depletion study. Clodronate/PBS liposomes are administered into the lateral ventricles 2 days before (pre-SAH treatment) or 3 hours after SAH induction. Neurobehavioral scoring was assessed 1, 2 and 5 days after SAH induction. Mice are sacrificed 5 days after SAH to observe degree of neuronal injury and perivascular inflammation after SAH; CL – Clodronate liposomes, PBSL – PBS liposomes. (e) Location of SAH burr hole relative to the location of the ventricular injection burr holes. (f) Clodronate depletes perivascular macrophages as demonstrated by absence of perivascular Iba-1 staining surrounding both transversely and longitudinally-cut vessels at 5 days after intraventricular clodronate injection (white arrows pointing to perivascular macrophages).

Blood injection model and tissue processing

CM-DiI-labelled red blood cells were injected by prechiasmatic injection as reported previously.[16] Briefly, animals were anesthetized with isoflurane (5% induction, 1.5–2% maintenance), carried by a mixture of oxygen and medical air (70:30 ratio, 1.5 L/min). A burr hole was made slightly right of the midline, 4.5 mm anterior to the bregma, with care to avoid the sinus. For the erythrocyte tracking

experiments, 100 µL of CM-DiI-labelled erythrocytes mixed with artificial CSF was injected into the prechiasmatic cistern through the burr hole at a 40° angle over 15 seconds with an injection pump. For the macrophage depletion experiments, whole blood from a littermate was used instead of labelled erythrocytes and injected in the same manner as the erythrocyte tracking experiment. Relative cerebral blood flow (CBF) monitoring was completed throughout the procedure with a Doppler flow meter (BLT21, Transonics Systems, New York, NY) to ensure proper SAH induction, as indicated by a sharp reduction in the CBF. Following SAH, mice were given slow release buprenorphine subcutaneously and recovered at 30 °C in an animal incubator. Welfare assessments were completed twice daily until day of sacrifice. At the time of sacrifice (either 10 minutes, 2 or 5 days), mice were transcardially perfused with 0.9% NaCl, followed by 4% paraformaldehyde (PFA) in phosphate-buffer (PB, pH = 7.4) (Figure 1(c)). Mice that were inadequately perfused were discarded from microthrombi analysis. For brain histology and visualization, brains were removed and stored in 4% PFA for 2 days, then transferred to 15% sucrose in PB for 4 hours, and then into 30% sucrose in PB overnight. Tissue was embedded in optimal cutting temperature compound (O.C.T., Sakura Finetek USA, Torrance, CA) and snap-frozen in cooled isopentane. For serial sectioning, 30 µm thick samples were sectioned in 500 µm intervals and mounted immediately with CC Mount™ (Millipore Sigma, St Louis, MO) after labelling with DAPI. Samples were sectioned cut between +2.00 mm to −4.50 mm relative to bregma. For immunofluorescence staining, sections were cut at 20 µm thickness, 1 mm from the bregma, and stored at −80°C until used.

Intraventricular administration of liposomes and FITC-dextran

Clodronate or PBS liposomes (Lipsoma, Netherlands) were injected into the lateral ventricles to deplete meningeal and perivascular macrophages, but not microglia (Figure 1(e) and (f)).[17,18] Animals were anaesthetized with isoflurane (5% induction, 1.5–2% maintenance), carried by a mixture of oxygen and medical air (70:30 ratio, 1.5 L/min). Mice were fixed to a stereotaxic frame, and 10 µL of clodronate or PBS liposomes were injected into each lateral ventricle over 12.5 minutes, using a Hamilton syringe attached to a pulled glass pipette (coordinates: AP −0.22 mm, lateral 1 mm, depth 2 mm). The pipette was left in place for 10 minutes after each injection to prevent backflow of liposomes through the injection path. For FITC-dextran labelling of perivascular macrophages, the same procedure was repeated for 10 µL of FITC-dextran (70 kDa, 0.1 mg/ml; Invitrogen, Carlsbad, D1823) in 5 mice. FITC-dextran was injected 2 days prior to the CM-DiI erythrocyte injection, and mice were sacrificed 5 days following erythrocyte injection.

Neurological scoring

Neurological function was assessed using a modified version of Garcia's score, as previously described.[19,20] The neurological assessment consists of 6 domains: spontaneous activity, spontaneous movement of all four limbs, forepaw outstretching, climbing, body proprioception and response to vibrissae touch. Spontaneous activity was measured by the time it took for the mouse to touch 3 walls with two paws, up to a maximum of 5 minutes. Two blinded observers conducted the neurological assessment before SAH induction and 1, 2 and 5 days after SAH induction. The maximum score is 18, indicative of normal neurological function.

Immunofluorescence staining

20 µm frozen sections were washed with PBS (pH = 7.40). Antigen was retrieved by incubation at 96 °C in citrate-based antigen retrieval solution (Vector Labs, Burlingame, CA) for 25 minutes. For intracellular labelling with antibodies, samples were permeabilized with 0.3% Triton X-100 in PBS for 1 hour. Samples underwent blocking in 10% goat serum with 1% BSA (in PBS, pH = 7.40). Samples were incubated with primary antibodies including rabbit anti-AQP-4 (1:400, EMD Millipore, AB3594), rabbit anti-GFAP (1:1000, Abcam, ab7260), rabbit anti-Iba-1 (1:1000, Wako, 019-19741) rabbit anti-caspase-3 (1:200, BD Pharmingen, 559565) or rabbit anti-fibrinogen (1: 1000, Abcam, ab34269) overnight at +4°C. After washing with PBS, secondary antibodies (goat anti-rabbit Alexa Fluor 488 (1:500) or goat anti-rabbit Alexa Fluor 568 (1:500)) targeted toward primary antibodies were placed on the slide and incubated at room temperature for 1 hour. For caspase-3 labelled samples only, tissue was then incubated with mouse anti-NeuN (1:200 Millipore, MAB377) antibody for 1 hour followed by goat anti-rabbit Alexa Fluor 568 (1:500) antibody for 1 hour. Samples were subsequently labelled with DAPI to reveal cellular nuclei and/or Alexa-633 hydrazide (2 nM) to label large arterioles and arteries where reported. Samples were mounted with CC/Mount™ (Millipore Sigma, St Louis, MO) and cover-slipped before imaging.

Fluorescence imaging

Samples were imaged using a whole slide scanner (Zeiss Axio Scan.Z1, Zeiss, Germany, 20X magnification, 40 ms exposure, with extended depth of focus) to

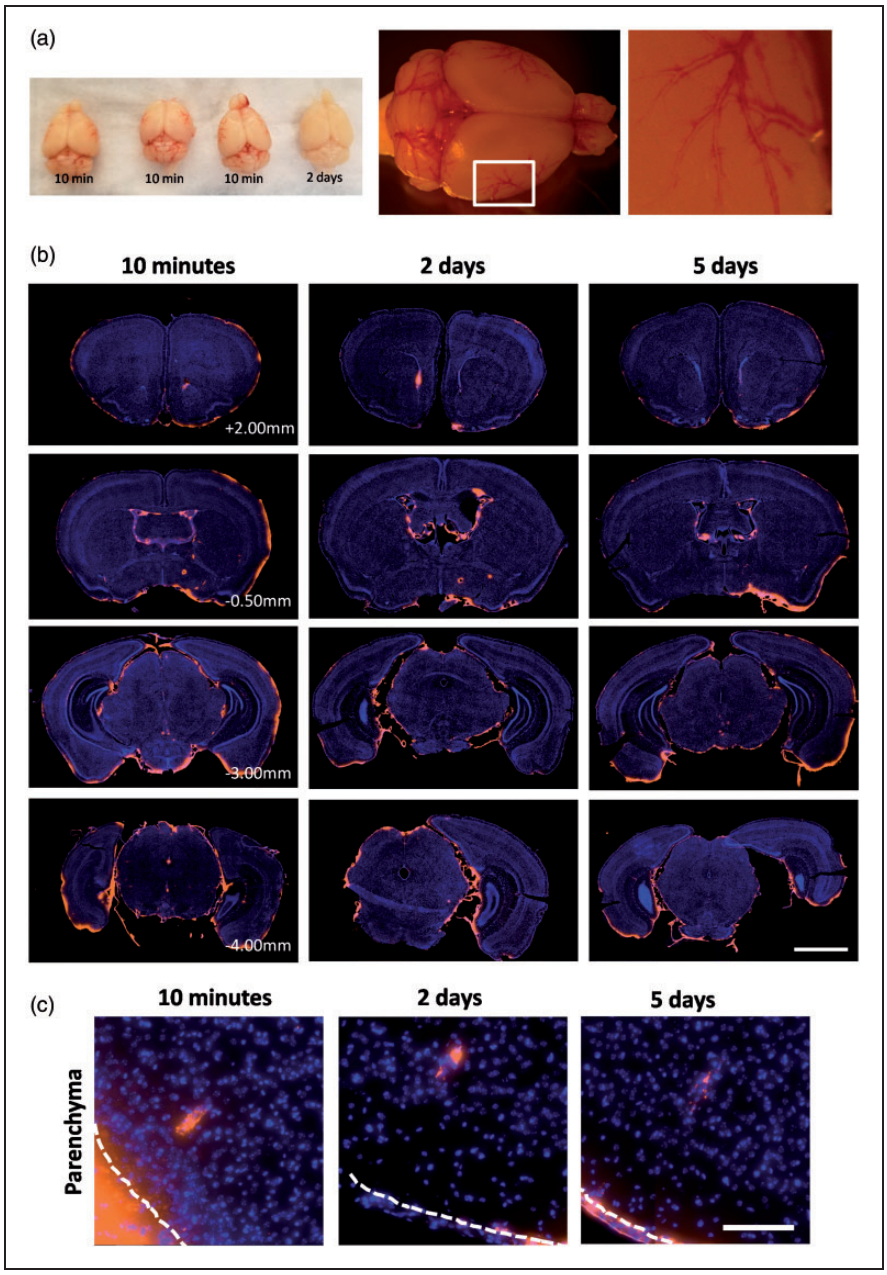

Figure 2. Macro- and microscopic distribution of erythrocytes after SAH. (a) Macroscopic images of mouse brains 10 minutes and 2 days after SAH. On the right is a mouse brain 10 minutes after SAH demonstrating macroscopic perivascular blood distribution. (b) Representative distribution of blood in the mouse brain in several coronal levels relative to bregma. Blood is labelled in orange, and nuclei are in the blue channel to highlight brain tissue (AP +2.00, +0.5 mm, –3.00 mm, –4.00 mm). Blood is distributed throughout the ventricular system and the base of the brain. Scale bar represents 2 mm (c) Dye can also be observed within the brain parenchyma at each time point, surrounding penetrating vessels. Note that dye appears to be contained in distinct cells at 2 and 5 days after SAH. White dotted line denotes the pia mater. Scale bar represents 250 μm.

visualize the distribution of CM-DiI label in the brain. For immunohistochemistry, samples were imaged using a confocal microscope (Zeiss LSM700, Zeiss, Germany) at 20X magnification. All images for each experiment were taken under the same imaging parameters immediately after immunolabelling. Images were processed using Zen2 blue software (Zeiss, Germany), IMARIS (Bitplane, Switzerland) and/or ImageJ (NIH, Bethseda, USA).

Image quantification

To quantify the depth from the brain surface that CM-DiI$^+$ cells were found, the orthogonal distance

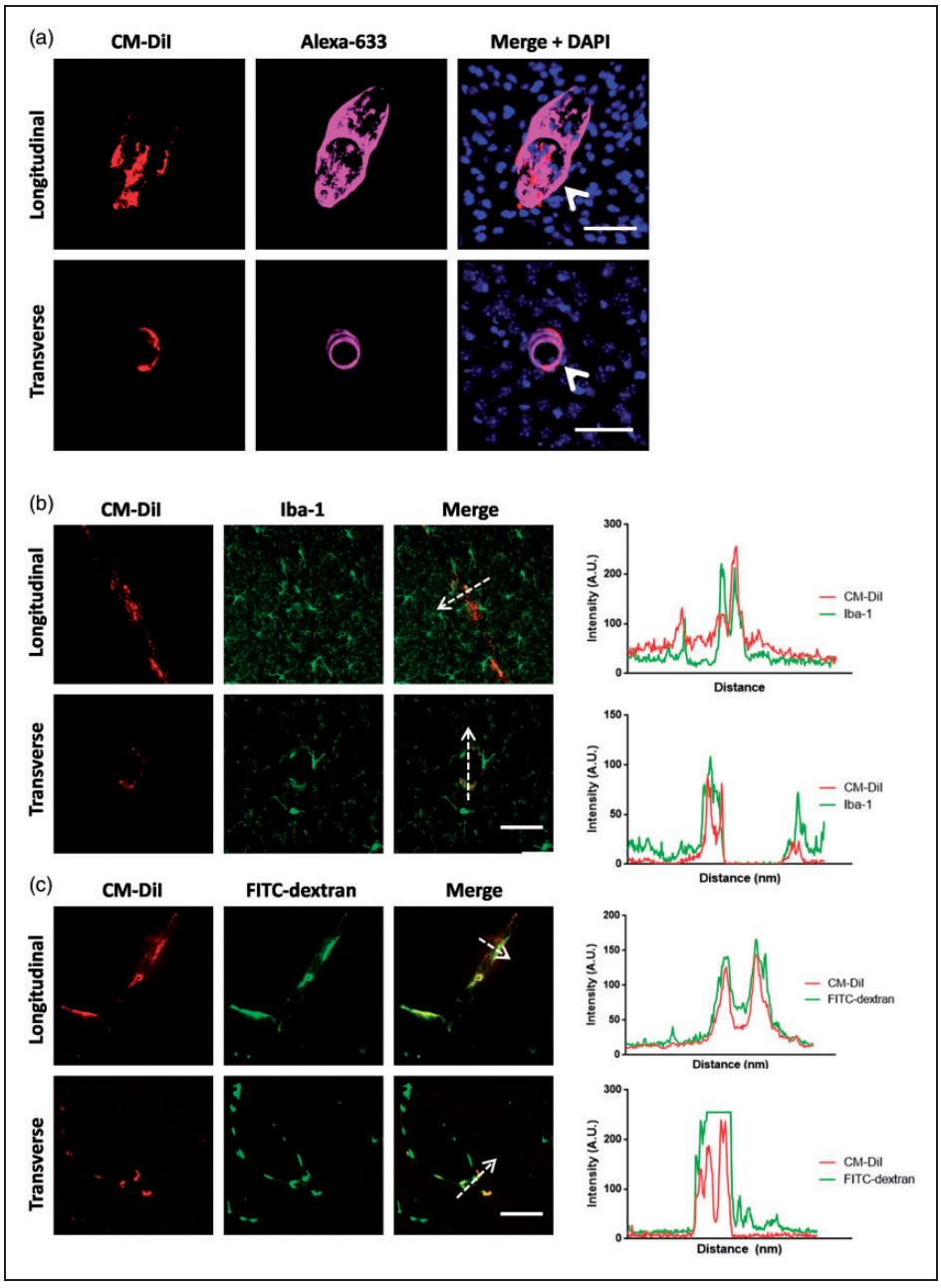

Figure 3. Distribution and identity of parenchymal perivascular CM-DiI$^+$ cells. These samples are stained at the 5 day time point. (a) The majority of parenchymal CM-DiI$^+$ cells were located along vessels that are labelled with Alexa-633, which specifically labels larger arterioles (>20 μm). Both longitudinally and transversely cut vessels with surrounding CM-DiI$^+$ cells were labelled with Alexa-633. Scale bar represents 50 μm (top row) or 20 μm (bottom row). (b) CM-DiI$^+$ cells (red) express relatively low levels of Iba-1 (green). Note the co-localization of CM-DiI with Iba-1 immunolabelling, along the direction of the dotted arrow. Scale bar represents 40 μm. (c) All CM-DiI$^+$ cells (red) were also involved in uptake of FITC-dextran (green). Note the co-localization of CM-DiI with FITC-dextran labelling, along the direction of the dotted arrow. Scale bar represents 40 μm. The perivascular location, low expression of Iba-1 (relative to surrounding microglia) and uptake of FITC-dextran indicate these cells are perivascular macrophages. Data are representative of n = 5 independent experiments.

from the surface of the brain to the deepest CM-DiI$^+$ cell surrounding the vessel was measured on whole slide images (Figure 3(a)). The depth of all CM-DiI$^+$ vessels on each serial slice was measured and reported as 'Depth from cortical surface'. In addition to collecting information about depth, the orientation of the vessel (transverse or longitudinal) relative to our coronal brain slice was also recorded. This was done for the

2 day and 5 day (n = 5), but not the 10 minute time point, as the intact erythrocytes had a tendency to detach from the slide during washing, preventing accurate quantification. To measure average GFAP expression around CM-DiI$^+$ vessels and control vessels, a mask was generated by thresholding the GFAP channel. The vessel surrounded by CM-DiI was traced by a blinded observer, and the positive area fraction within the traced area was reported as 'GFAP coverage'. For caspase-3, microthrombi and GFAP$^+$ vessel quantification, a single coronal slice from the bregma was used for quantification. All NeuN$^+$ cells containing caspase-3 signal and GFAP$^+$ vessels were counted on each slice by a blinded observer. Microthrombi were counted in 12 fields per brain slice at 20X magnification and normalized by total area scanned.

Statistical analysis and exclusions from analysis

For normal continuous data, a Student's t-test was used for comparisons of unpaired data and a paired t-test for paired data. For ordinal data or non-normally distributed data (i.e., neurobehavioral scores), a Mann Whitney-U test was used. Normality was tested by the Shapiro-Wilk normality test. P-values of <0.05 were considered to be significant. For categorical data, a Fisher's exact test was used. Continuous data are reported as means ± standard deviation (SD) and ordinal or non-normal data are reported as medians ± interquartile range (IQR). 1 mouse was excluded in the microthrombi analysis from the post-SAH clodronate-liposome group, and 1 mouse from the pre-treated PBS-liposome group for incomplete perfusion. Lastly, mice in the pilot group were not used for histology, as behavior was not assessed, and brains were not perfused with fixative. Hence only clot burden was evaluated from these mice.

Results

Spatial and temporal profile of CM-DiI labelled erythrocytes after SAH

To determine the location of erythrocytes in the prechiasmatic injection model, we labelled erythrocytes with CM-DiI and then injected them. 10 minutes after prechiasmatic injection, erythrocytes were macroscopically distributed around the perivascular space of the middle cerebral artery and also within the subarachnoid space (Figure 2(a)). We observed the perivascular erythrocytes to be slightly more pronounced on the side ipsilateral to the burr hole, which was slightly off the midline (Burrhole location, Figure 1(e)). In the posterior brain, we noted localization of erythrocytes surrounding the cerebellar arteries. No erythrocytes were observed macroscopically in the perivascular spaces at either the 2 or 5 day time-points (5 day not shown).

To visualize the microscopic distribution of erythrocytes after SAH, brains were sectioned at 500 μm intervals and slices were imaged using a whole slide scanner (Figure 2(b)). At all time points, CM-DiI containing (CM-DiI $^+$) cells were present throughout the ventricular system, and particularly pronounced near the injection site (Supplemental Figure 2). These cells were also found on the leptomeninges underneath the brain and surrounding the brainstem. At 10 minutes, CM-DiI$^+$ cells were intact erythrocytes, but by 2 and 5 days, most of the dye was found localized in elongated spindle or round-shaped mononuclear cells in the subarachnoid space and ventricles (Supplemental Figure 2). The leptomeningeal cells, based on their localization, shape, single nucleus and propensity to uptake erythrocytes were identified as meningeal macrophages. In addition to the subarachnoid space and ventricles, we found CM-DiI signal surrounding parenchymal vessels (Figures 2(c) and 4(b)). Similar to the ventricular and leptomeningeal distribution, at 10 minutes, parenchymal perivascular CM-DiI$^+$ cells were intact erythrocytes, but by 2 and 5 days, most of the dye was found localized in discrete elongated spindle shaped cells. The vessels with surrounding CM-DiI$^+$ cells were running parallel or transversely relative to the coronal plane of sectioning. Aside from these cells in the perivascular space, no other cells containing dye were found within the parenchyma.

Identification and localization of parenchymal perivascular CM-DiI$^+$ cells

To better understand the distribution of parenchymal perivascular CM-DiI$^+$ cells, we investigated the type of vessels that these cells surrounded. We incubated brain slices with Alexa Fluor 633 hydrazide, which selectively labels elastin surrounding large arterioles.[21] We found that all transversely cut vessels and the majority of longitudinally cut vessels with surrounding CM-DiI$^+$ cells were co-labelled with Alexa-Fluor 633 (Figure 3(a)). This indicated that the majority of parenchymal CM-DiI$^+$ cells were perivascular cells surrounding large penetrating arterioles.

Given the location and morphology (perivascular distribution around arterioles, spindle shaped) of the CM-DiI$^+$ cells 2 and 5 days following SAH, we hypothesized that these were perivascular macrophages. To confirm this, we stained the tissue for Iba-1, a macrophage/microglia marker. We found that CM-DiI$^+$ cells had a low baseline expression of Iba-1 which is consistent with perivascular macrophages and not parenchymal microglia (Figure 3(b)).[22,23] Furthermore, we did not observe any parenchymal microglia (Iba-1$^+$ cells in

the parenchyma) that were also CM-DiI$^+$ (Figure 3(b)). In a separate cohort of mice we administered intraventricular FITC-dextran, which is specifically phagocytosed by perivascular macrophages, 2 days prior to CM-DiI erythrocyte injection.[22,23] We found that all CM-DiI$^+$ cells also contained FITC-dextran (Figure 3 (c)). Together, the morphology, location, relative Iba-1 expression and FITC-dextran uptake indicate these cells are perivascular macrophages.

Distribution pattern of perivascular CM-DiI$^+$ macrophages after SAH

We subsequently assessed the distribution of CM-DiI$^+$ perivascular macrophages throughout the mouse brain to estimate the extent of parenchymal perivascular infiltration of blood (Figure 4). On visual inspection of the anterior slices at low magnification, we observed that there were slightly more CM-DiI$^+$ perivascular macrophages lateralized towards the side of the injection consistent with the pattern of macroscopic perivascular blood distribution (Figure 4(a)). The majority of vessels with surrounding CM-DiI$^+$ macrophages (i.e., 'CM-DiI$^+$ vessels') on these anterior slices were cut longitudinally with the coronal slice, running perpendicular to the brain surface (Figure 3(e)). On visualization of the posterior slices at low magnification, the CM-DiI$^+$ vessels were found to be distributed more evenly along both sides of the cortex (Figure 4(a)). In these more posterior sections, vessels that were cut transversely with the coronal slice (i.e., running parallel to the brain surface) became more common (Figure 4 (e)). We then quantified the depth at which these CM-DiI$^+$ vessels were found relative to the brain surface, distinguishing between transverse and longitudinally-cut vessels.

The longitudinal vessels originated from the brain surface, and the CM-DiI$^+$ cells along these vessels were found deep in the brain parenchyma - as deep as 1 mm from the brain surface - with an average depth of 0.43 ± 0.38 and 0.38 ± 0.30 mm in the 2 and 5 day time-points respectively (Figure 4(c) and (d)). The transversely-cut CM-DiI$^+$ vessels were typically found deeper in the brain tissue, in the posterior brain. These vessels were found within the posterior hippocampus, and other sub-cortical structures (Figure 4(c) and (d)). Transverse vessels were found as deep as 2.5 mm from the cortical surface, with an average depth of 1.39 ± 0.55 mm and 1.29 ± 0.50 mm from the cortical surface at 2 and 5 days following SAH induction. The pathway by which erythrocytes enter the perivascular space of the deeper transverse vessels is unclear. Comparing between 2 and 5 days post-ictus, there were less vessels with surrounding CM-DiI$^+$ cells at 5 days compared to 2 days (15.2 vs. 10.1 vessels/slice), indicating a possible turnover or clearance of perivascular macrophages over time (Figure 4(e)). These data indicate that perivascular blood is not only in the superficial cortex, but also deeper cortical and subcortical regions.

CM-DiI$^+$ perivascular macrophages are associated with increased perivascular gliosis

To determine if the presence of blood and perivascular macrophages initiated an inflammatory response in the surrounding tissue, we stained brain slices for GFAP, to detect reactive gliosis.[24] We observed that around blood vessels with CM-DiI$^+$ macrophages, there was increased expression of GFAP in neighbouring astrocytes which is indicative of reactive gliosis (Figure 5). To estimate the increased expression, we measured the GFAP coverage of the vessel wall, comparing similar sized vessels that had surrounding CM-DiI$^+$ macrophages with those that were CM-DiI$^-$. In terms of the total vessel area coverage, we found an average increase in GFAP expression of $17.7 \pm 3.8\%$ relative to control non-labelled vessels ($P < 0.001$, paired t-test) at 2 days after SAH. GFAP was found to further increase at the 5 days ($29.4 \pm 19.4\%$ increase vs. non-labelled vessels, $P < 0.05$, paired t-test). In addition to increased GFAP expression, we observed that expression of aquaporin-4 (AQP4), which is typically found on the end-feet of perivascular astrocytes, appeared disrupted or absent in comparison to vessels that were not surrounded by CM-DiI$^+$ cells (Supplemental Figure 3). These data indicate that perivascular blood and/or the perivascular macrophages that uptake the blood may cause reactive gliosis and local neurovascular inflammation. A summary of findings in the erythrocyte tracking experiments are presented in Figure 5(b).

Depletion of perivascular and meningeal macrophages affects behavioural deficits and delays blood clearance after SAH

Next, to study how perivascular and meningeal macrophages influence the response to SAH, we used clodronate liposomes to deplete these cell populations (Figure 1(d)). For these experiments, whole blood was used. Clodronate liposomes specifically induce apoptosis in leptomeningeal and perivascular macrophages without affecting microglia, achieving almost complete depletion by 2 days after injection.[13] Successful depletion of perivascular and meningeal macrophages in our study was indicated by an absence of perivascular Iba-1 staining (Figure 1(f)). Depletion was initiated 2 days before SAH (i.e. pre-SAH treatment) or 3 hours after SAH (post-SAH treatment).

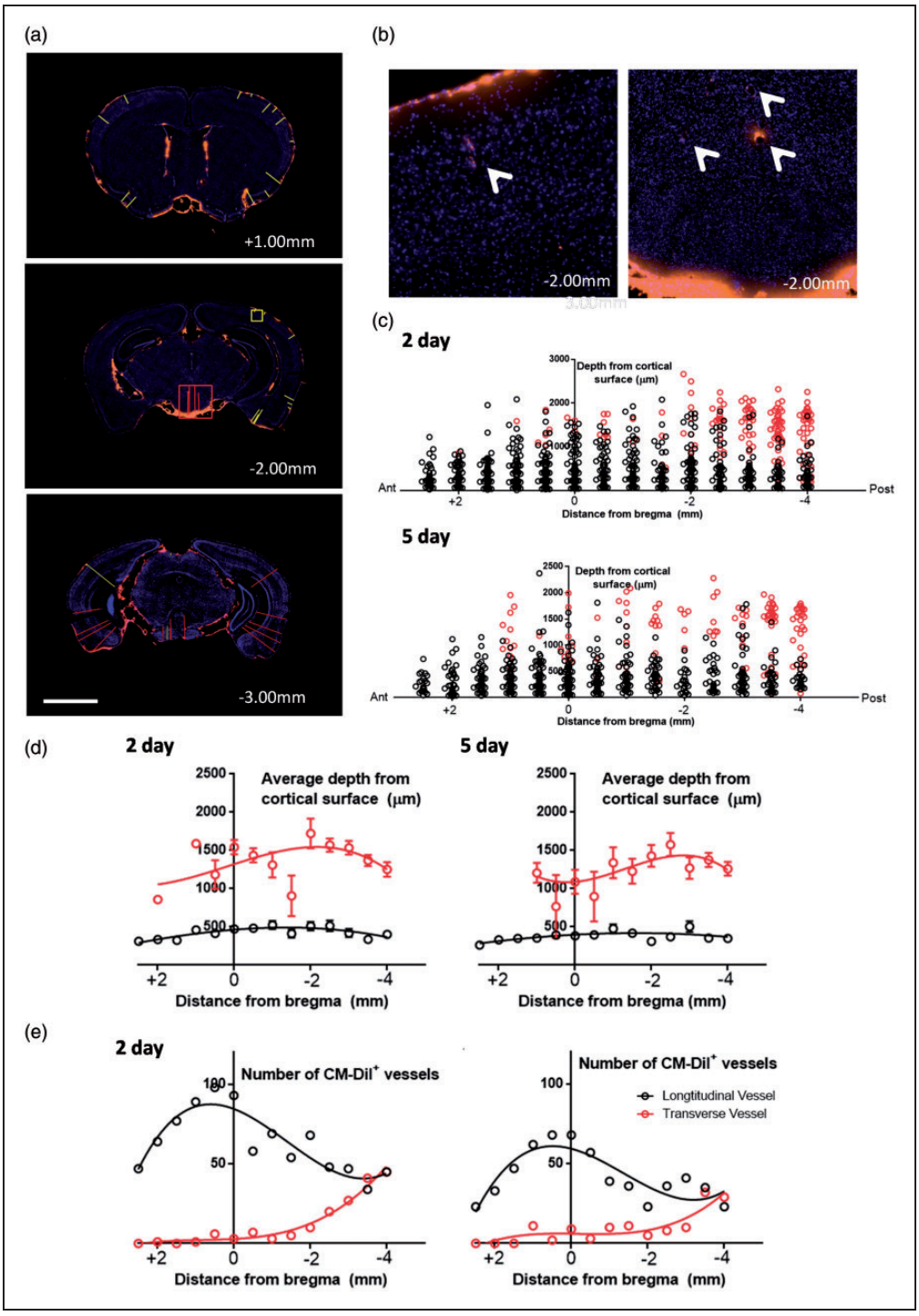

Figure 4. Distribution of perivascular CM-DiI$^+$ macrophages after SAH. (a) Representative coronal slices obtained 2 days after SAH, at +1.00 mm, −2.00 mm, and −3.00 mm from the bregma. Red lines indicate distance from cortical surface to a vessel that was perpendicular to the coronal cut (i.e., transverse vessel), and yellow lines indicate distance from cortical surface to a vessel that was parallel to the coronal cut (i.e., longitudinal vessel). Note that longitudinally-cut vessels with perivascular CM-DiI$^+$ cells were found more often on the ipsilateral slide to the side of burr hole (right of mouse, left side of image), particularly towards the anterior brain. Scale bar represents 2 mm. (b) Inset of two regions from second slice in A (AP −2.00 mm) or a longitudinal vessel (inset of yellow box, right figure) or transverse vessel (inset of red box, left figure). (c) Graphical representation of the spatial distribution of cortical vessels with surrounding perivascular CM-DiI$^+$ macrophages. Red circles indicate transversely-cut vessels, and black circles indicate longitudinally-cut vessels. (d) Summary data of the average cortical depth of transverse or longitudinal arterioles in various brain slices at 2 (left) or 5 (right) days. Note that transversely-cut vessels were typically found in deeper cortical regions than longitudinally-cut vessels. Data are expressed as means ± standard deviation. (e) Summary data of the total number of vessels that had surrounding perivascular CM-DiI$^+$ macrophages. Note that the number of vessels peaked around the level of the bregma for longitudinally-cut vessels, whereas the number of transversely-cut vessels increases progressively towards the posterior sections. Curves of best fit are applied for data visualization. Data are obtained from n = 5 mice per time point in each graph from (d-e).

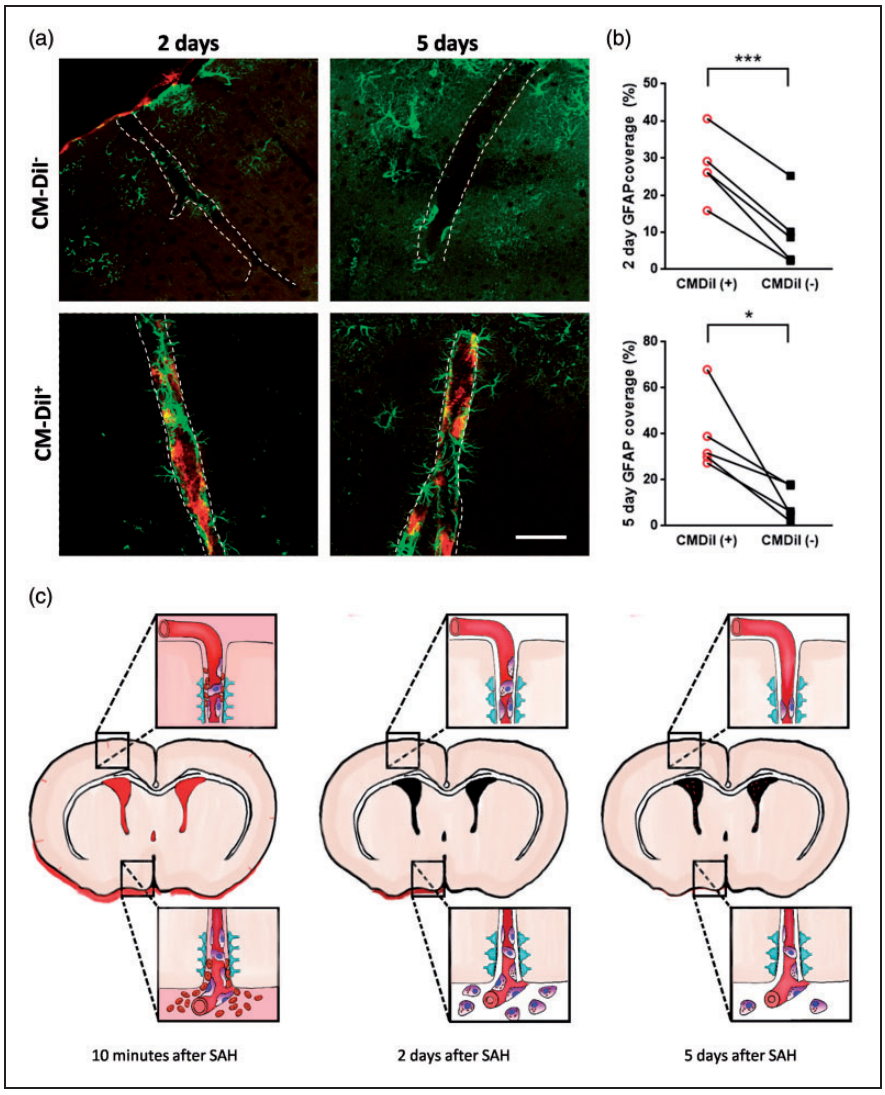

Figure 5. Gliosis surrounding blood vessels with perivascular CM-DiI^{+} macrophages and primary findings of erythrocyte tracking experiments. (a) Representative images of cortical blood vessels (highlighted with the dotted line), stained with GFAP, a specific marker of astrocytes. Increased GFAP expression (green) is associated with inflammation and gliosis. No significant gliosis was observed surrounding CM-DiI^{-} vessels. In contrast, we observed a large increase in the perivascular GFAP expression surround blood vessels labelled with perivascular CM-DiI^{+} cells (red). Scale bar represents 30 μm. (b) Quantification of perivascular gliosis. CM-DiI^{+} vessels were compared to CM-DiI^{-} vessels in the same animal for both 2 and 5 days after SAH. ***$P < 0.0001$, *$P < 0.05$, paired t-test (n = 4 independent samples/group). (c) Schematic of the primary findings in the erythrocyte tracing studies. At 10 minutes, free intact erythrocytes were found in the basal cisterns and ventricles. Intact erythrocytes were also found in the perivascular spaces of apical, basal and subcortical arterioles. At 2 days after SAH, there was decreased blood and erythrocytes in the basal cistern. Blood in the ventricles was phagocytosed by discrete cells. Erythrocyte uptake was observed by perivascular and meningeal macrophages (in purple) but not microglia. Perivascular gliosis was observed primarily around arterioles with perivascular macrophages that engaged in erythrocyte clearance (swollen endfeet, in blue). At 5 days after SAH, little or no blood was found in basal cisterns. Blood in the ventricles were contained by discrete cells. Some turnover of the perivascular macrophages and more perivascular inflammation were observed. Overall, we found that perivascular and meningeal macrophages are involved in erythrocyte clearance, and contribute to perivascular inflammation and neuronal cell death after SAH. Note that erythrocytes, macrophages and astrocytic endfeet are not drawn to scale.

We found that clodronate pre-treatment had no effect on neurological scoring on the modified Garcia's score in comparison to PBS pre-treated mice, at any time-point ($p > 0.05$, Mann-Whitney-U) (Figure 6(a)). In contrast with the clodronate pre-treated animals, animals treated after SAH had improved neurological scores at all time-points in comparison to PBS treatment ($P < 0.05$, Mann-Whitney-U t-test) (Figure 6(b)). Mice were sacrificed after behavioural testing on day 5, at which time we observed coagulated blood still present

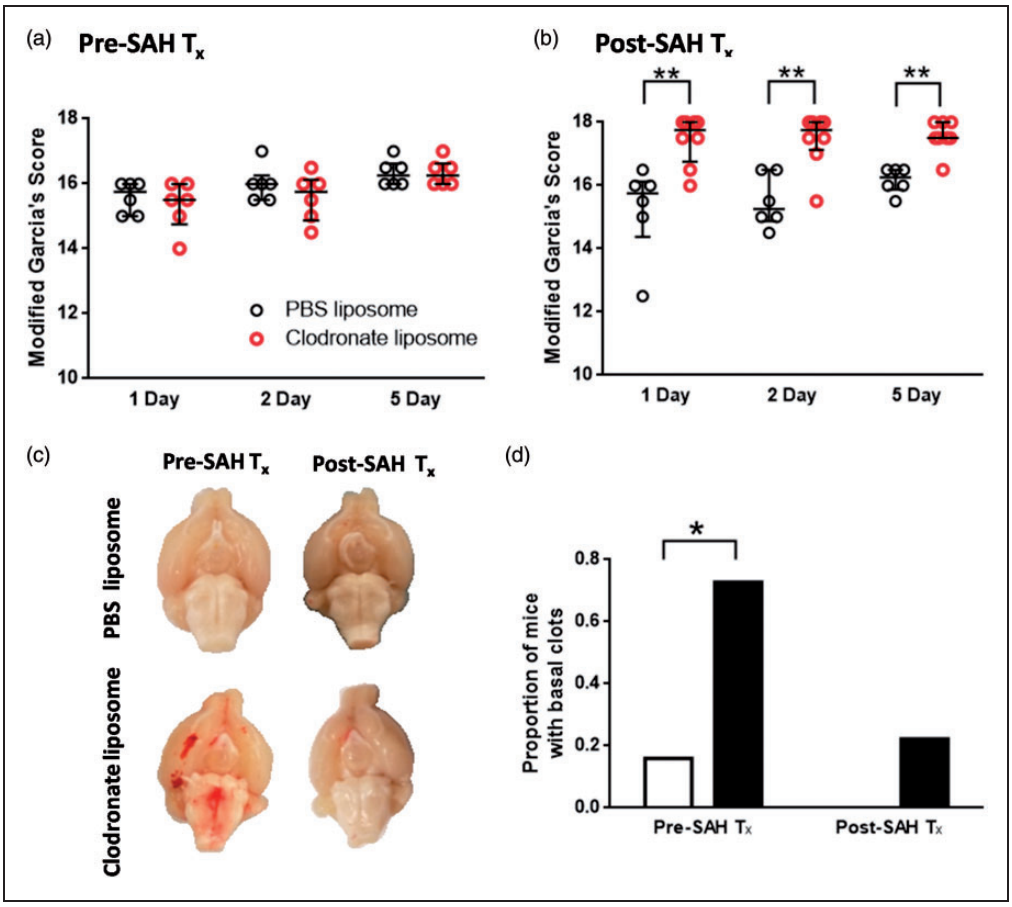

Figure 6. Depletion of perivascular and meningeal macrophages affects gross behaviorial deficits and blood load after SAH. (a) (a) Neurological scoring of mice receiving pre-SAH treatment with clodronate or PBS liposomes. No difference in behavioural scoring was observed between the PBS and clodronate groups. (b) Neurological scoring of mice receiving post-SAH treatment of clodronate or PBS liposomes (n = 6 mice per group). Clodronate-treated mice scored significantly better in neurobehavioural scoring compared to the PBS-treated controls (*$P < 0.05$, **$P < 0.01$, Mann-Whitney-U test). (c) Representative ventral view of the brain surface of clodronate or PBS treated mice, sacrificed at 5 days after SAH. Typically, no blood is observed on the ventral brain surface by 5 days after SAH, but after clodronate pre-treatment, there was a clear basal clot in a significant proportion of mice compared with controls (quantified in (d), * $P < 0.05$, Fisher's exact test).

in the basal cisterns in mice that received the clodronate pre-treatment, but not those pre-treated with PBS liposomes (Figure 6(c)). Some clodronate post-treated mice also had small amounts of clotted blood in the basal cisterns, but not a significantly higher number than PBS treated controls ($P < 0.05$, Fisher's exact test, pre-treatment group (clodronate 8 of 11, PBS 1 of 6 had clots); same day group (clodronate 2 of 9, PBS 0 of 6 had clots)) (Figure 6(d)).

Depletion of perivascular and meningeal macrophages affects neuronal injury after SAH

Since mice had improved behavioural scoring after simultaneous clodronate and SAH injection, we measured the effect of macrophage depletion on neuronal injury after SAH using caspase-3/NeuN staining. Caspase-3 staining was quantified from the cerebral cortices of a single slice. Caspase-3 distribution was highest in the cortical tissue adjacent to the subarachnoid blood clot, with scattered distribution in the other regions of the cerebral cortex (Figure 7(a)). In pre-SAH treated animals we did not detect a significant decrease in the number of caspase-3^+ neurons between clodronate or PBS treated animals (225 ± 151 vs. 161 ± 129 neurons, $p > 0.05$, Student's t-test) (Figure 7(d)). Contrastingly, in animals treated post-SAH, we observed a significant reduction in the number of caspase-3^+ neurons compared to PBS controls (186 ± 78 vs. 56 ± 48 neurons, $P < 0.01$, Student's t-test).

Depletion of perivascular and meningeal macrophages reduces inflammation surrounding large arterioles and reduces microthrombosis after SAH

Lastly, to determine if macrophage depletion reduced perivascular inflammation, we quantified the total

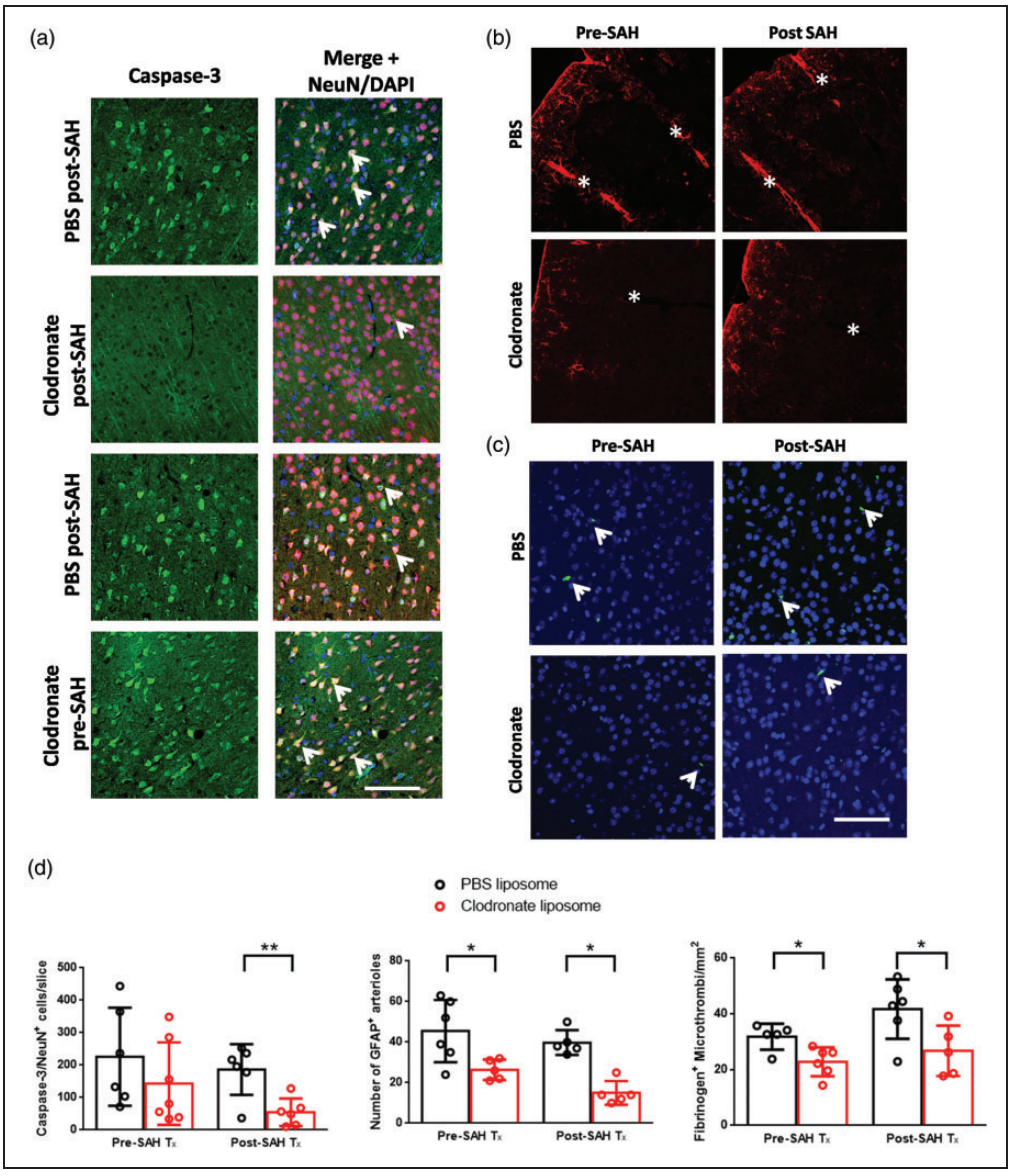

Figure 7. Depletion of perivascular and meningeal macrophages affects neuronal cell death, perivascular gliosis and microthrombosis after SAH. (a) Representative images of caspase-3 (green) staining in PBS or clodronate treated mice. Images are merged with NeuN (red) and DAPI (blue). Positive cells are yellow in the merge (white arrows). (b) Representative GFAP staining visualizing astrocyte activation surrounding penetrating vessels after SAH in PBS or clodronate treated animals. Vessels are indicated with a white asterisk, and are identified by the presence of a vascular lumen. (c) Representative images of fibrinogen staining (green), with DAPI (blue) in PBS or clodronate treated mice. d) Quantification of neuronal cell death, perivascular gliosis and thrombosis in clodronate or PBS-treated animals. Neuronal cell death was only significantly reduced in SAH animals treated with clodronate vs. PBS controls treated on the same day. In both pre-SAH and post-SAH treated clodronate-treated SAH animals, the number of $GFAP^{+}$ arterioles and number of thrombi was significantly reduced vs. PBS-treated animals from the same cohort, $^{*}P < 0.05$, $^{**}P < 0.01$, Student's t-test, n = 5-6 per group. Scale bars: (a) 50 μm, (b,c) 60 μm.

number of large penetrating vessels that had visible expression of GFAP in clodronate-treated and PBS-treated mice (Figure 7(b)). Interestingly, we found that, in both mice that received clodronate on 2 days prior to SAH and on the same day as SAH, there was a significant reduction in the total amount of GFAP immunoreactivity surrounding large arterioles in comparison to PBS-treated controls (pre-SAH treatment: 45.5 ± 15.3 vs. 26.4 ± 5.0 arterioles, $P < 0.05$, Student's t-test; post-SAH treatment, 39.8 ± 6.1 vs. 15.0 ± 5.8 arterioles, $P < 0.05$, Student's t-test) (Figure 7(d)).

Given this reduction in perivascular inflammation, we sought to quantify the degree of microthrombosis in

each group, as the formation of microthrombi has been linked to vascular inflammation after SAH.[25,26] Consistent with a potential reduction in perivascular inflammation, there was a reduction in the number of microthrombi/mm^2 in both clodronate-treated groups, compared to the respective PBS-treated group (pre-SAH treatment: 32 ± 5 vs. 23 ± 5 microthrombi/mm^2, $P < 0.05$, Student's t-test; post-SAH treatment, 42 ± 11 vs. 27 ± 9 microthrombi/mm^2, $P < 0.05$, Student's t-test) (Figure 7(c) and (d)).

Discussion

This study had several important new findings which are critical to the understanding of blood clearance and evolution of brain injury after SAH. We confirmed that erythrocytes were distributed throughout the subarachnoid space after SAH, predominantly near the site of injection, which importantly shows consistency with human aneurysmal SAH (Figure 5(b)). In addition, intact erythrocytes are present in the leptomeninges and perivascular spaces. We found that these erythrocytes were primarily cleared by perivascular and meningeal macrophages and not microglia. Lastly, we demonstrated that depletion of perivascular and meningeal macrophages using clodronate liposomes improved outcome after SAH, but only in animals that were treated on the same day post-SAH, but not two days prior to SAH. To the best of our knowledge, the current work is the first to describe the spatial distribution of perivascular erythrocytes, and show the pathophysiological importance of perivascular and meningeal macrophages in erythrocyte clearance and outcome after SAH.

The distribution of CM-DiI-containing cells indicate that erythrocytes are present throughout the subarachnoid space, and enter the Virchow-Robin/perivascular spaces immediately after SAH. The erythrocytes in the perivascular space are presumably trapped until they are removed by local perivascular macrophages. The distribution of the labelled perivascular macrophages was preferentially ipsilateral to the injection side on the anterior slices, and evenly distributed bilaterally in the posterior slices, which mirrors the macroscopic surface distribution of blood. Interestingly, we found evidence of erythrocytes in perivascular spaces deep into the brain parenchyma, particularly around vessels running parallel to the brain surface. It is unclear how erythrocytes can enter into the perivascular space of these deeper arterioles, though they were found in more posterior brain slices. This suggests that perivascular blood may not only directly affect superficial cortical brain tissue, but also deeper cortical/sub-cortical structures, such as the hippocampus which experience pathological changes after SAH.[27] Though the detailed characterization of blood distribution after experimental SAH has not been previously reported, other groups have found evidence of erythrocytes and/or blood products in Virchow-Robin spaces after SAH.[13,14] In a rat cisterna magna injection model of SAH, erythrocytes were found surrounding penetrating arterioles at both 10 minutes and 4 days after SAH, as deep as 500 μm into the parenchyma.[28] More recently, Luo et al. (2016) injected blood mixed with a fluorescent-labelled dextran and observed plasma entering into the subarachnoid space immediately after SAH, which diffused into the perivascular space over one hour.[11] Additionally, they found intact erythrocytes in the perivascular space in post-mortem SAH patients, indicating blood may enter the perivascular space in humans. Lastly, in a primate model of SAH, fibrinogen was observed in the perivascular space, indicating the presence of extravascular blood, though no intact erythrocytes were observed in the study.[14]

We found that cells expressing CM-DiI at 2 and 5 days were perivascular or meningeal macrophages, which are a unique macrophage population that can be genetically distinguished from parenchymal microglia and other central nervous system macrophage populations.[29,30] In our study, we did not identify parenchymal microglia that were CM-DiI$^+$, indicating that they did not engage in erythrophagocytosis. These data challenge the notion that the erythrophagocytosis is mediated by parenchymal microglia as proposed by Schallner et al. (2015) and Kaiser et al. (2020).[9,11] They found that mice lacking heme-oxygenase-1 (HO-1) in microglia had impaired ability to clear blood and heme from the subarachnoid space. Furthermore, microglia had significantly increased expression of HO-1 after SAH, suggesting that they had a role in the clearance of blood after SAH. However, the expression of HO-1 was not evaluated in other central nervous system macrophage populations, and the macrophage-specific genetic targeting of HO-1 was not specific to microglia. Based on our present results, it appears that perivascular and meningeal macrophages are more involved in direct clearance of erythrocytes while microglia may play a supportive role. Furthermore, based on their anatomical location, meningeal and perivascular macrophage subpopulations should be the first to interact with erythrocytes and other blood products and hence may also be responsible for initiating the parenchymal inflammatory response after SAH. Consistent with this hypothesis, paravascular brain regions adjacent to CM-DiI$^+$ vessels displayed high levels of gliosis in comparison to regions adjacent to CM-DiI$^-$ vessels.

To determine if perivascular and meningeal macrophages influence outcome after SAH, we depleted these macrophage subpopulations before or after SAH. Our results suggest that there may be a dual role for

perivascular and meningeal macrophages in influencing outcome after SAH. Early pre-SAH depletion of these macrophages resulted in increased blood load at 5 days post-ictus and an absence of histological and behavioural neurological recovery. In contrast, delayed depletion of macrophages significantly reduced neuronal apoptosis and improved neurological scoring, and did not increase the blood load. However, in both clodronate-treated groups, we found reduced signs of perivascular inflammation as indicated by perivascular gliosis. Lastly, perivascular inflammation has been associated with the formation of microvascular thrombi, an important contributor to DCI after SAH.[25,26] Consistent with the reduction in perivascular inflammation, in both the clodronate treated groups, there was a reduction in microthrombosis. Together, these data indicate that perivascular macrophages increase perivascular inflammation after SAH, though the molecular mechanism by which this occurs is still unclear. Based on studies on other CNS macrophages, the increased inflammatory response could be due to increased nitric oxide (NO) production, as blood products enhance expression of inducible NO synthase.[31] The potential neuroprotective benefit of reduced perivascular inflammation in pre-treated mice may be reduced by the delayed clot clearance, which is correlated to poor outcome in rodent models.[32,33] The dual role of perivascular macrophages in modulating injury has been previously described in Alzheimer's disease. Perivascular macrophages are critical for the clearance of amyloid beta (Aβ) plaques, and depletion of perivascular macrophages significantly increases the plaque load in the TgCRND8 mouse model.[34] However, the phagocytosis of Aβ also promotes the production of reactive oxygen species in perivascular macrophages which results in increased perivascular inflammation and cerebrovascular dysfunction.[35] Similarly, in the mice treated prior to SAH, though there may be a reduced inflammatory burden due to the macrophage depletion, the negative effects of increased blood breakdown product in the subarachnoid/perivascular spaces may obscure the functional benefit. Contrastingly, the delayed administration of clodronate may allow perivascular macrophages to uptake the blood, but are depleted before they can inflict significant perivascular injury.

This study has several limitations. Firstly, we cannot confirm that all the fluorescent dye injected into the subarachnoid space was bound to erythrocytes, and that perivascular and meningeal macrophages consumed labelled erythrocytes rather than free dye. However, DiI and its derivatives are lipophilic cationic indocarbocyanine dyes, and readily intercalate into the outer leaflet of cell membranes.[36] If the dye was freely diffusing through the CSF, the small molecular weight dye would theoretically diffuse throughout the glymphatic system and label capillaries and venules, if it exists.[37,38] The relatively specific labelling of perivascular and meningeal macrophages therefore indicates a specific uptake of erythrocyte-bound dye. Another limitation is that erythrocytes were injected into the subarachnoid space in the first part of our study rather than whole blood. Importantly, other blood cells and blood products are involved in the pathogenesis of DCI and early brain injury. In particular, injection of platelet rich plasma into the subarachnoid space has been shown to induce vasospasm of large arteries in non-human primates and canines.[39,40] Other blood products such as clotting factors may also allow erythrocytes to persist longer within the subarachnoid space rather than being rapidly engulfed by perivascular and meningeal macrophages. Indeed, in prior studies, intact erythrocytes were detected as late as 4 days after SAH.[28] Repeating the experiment with whole blood or other labelled blood products may reveal further information about the perivascular and meningeal macrophage response to blood. Lastly, recirculation of labelled erythrocytes may have confounded our interpretation. After injection of erythrocytes in the subarachnoid space, some will re-enter the central circulation as they are drained through the arachnoid granulations into the dural sinuses. If there is severe enough blood brain barrier disruption, these fluorescent blood cells could enter the perivascular space through the central circulation, and be subsequently uptaken by perivascular macrophages.[41]

Our work here demonstrates erythrocytes are found in the subarachnoid space, can enter into the arteriolar perivascular space after SAH, and are consumed by perivascular and meningeal macrophages. Based on the cells that were engaged in CM-DiI uptake, microglia did not appear to be directly involved in erythrocyte clearance, though we did not exclude the possibility of a supportive role. Depletion of meningeal and perivascular macrophages may have a neutral or beneficial effect depending on the timing of the depletion. Future work is required to determine the specific molecular mechanisms by which these macrophage subpopulations influence outcome after SAH.

Funding

The author(s) disclosed receipt of the following financial support for the research, authorship, and/or publication of this article: Supported by grants from Heart and Stroke Foundation to RLM and the Brain Aneurysm Foundation (Running Against Ruptures — Bob Wood Chair of Research and Donald Sutherland Chair of Research) to JA and RLM.

Declaration of conflicting interests

The author(s) declared no potential conflicts of interest with respect to the research, authorship, and/or publication of this article.

Authors' contributions

HW, KH, RLM contributed to the conception and experimental design.
HW, SB performed experiments, analyzed data, and interpreted the experimental results.
JA analyzed data and interpreted the experimental results.
HW drafted the manuscript.
All authors edited, revised the manuscript and approved the final manuscript.

Supplementary material

Supplemental material for this paper can be found at the journal website: http://journals.sagepub.com/home/jcb

References

1. Sandvei MS, Romundstad PlR, MüLler TommBrostrup, et al. Risk factors for aneurysmal subarachnoid hemorrhage in a prospective population study: the HUNT study in Norway. *Stroke* 2009; 40: 1958–1962.
2. Rivero-Arias O, Gray A and Wolstenholme J. Burden of disease and costs of aneurysmal subarachnoid haemorrhage (aSAH) in the United Kingdom. *Cost Eff Resour Alloc* 2010; 8: 6.
3. Fujii M, Yan J, Rolland WB, et al. Early brain injury, an evolving frontier in subarachnoid hemorrhage research. *Transl Stroke Res* 2013; 4: 432–446.
4. Macdonald RL. Delayed neurological deterioration after subarachnoid haemorrhage. *Nat Rev Neurol* 2014; 10: 44–58.
5. Rowland MJ, Hadjipavlou G, Kelly M, et al. Delayed cerebral ischaemia after subarachnoid haemorrhage: looking beyond vasospasm. *Br J Anaesth* 2012; 109: 315–329.
6. Joerk A, Ritter M, Langguth N, et al. Propentdyopents as heme degradation intermediates constrict mouse cerebral arterioles and are present in the cerebrospinal fluid of patients with subarachnoid hemorrhage. *Circ Res* 2019; 124: e101–e114.
7. Clark JF and Sharp FR. Bilirubin oxidation products (BOXes) and their role in cerebral vasospasm after subarachnoid hemorrhage. *J Cereb Blood Flow Metab* 2006; 26: 1223–1233.
8. Lee JY, Keep RF, He Y, et al. Hemoglobin and iron handling in brain after subarachnoid hemorrhage and the effect of deferoxamine on early brain injury. *J Cereb Blood Flow Metab* 2010; 30: 1793–1803.
9. Schallner N, Pandit R, LeBlanc R, et al. Microglia regulate blood clearance in subarachnoid hemorrhage by heme oxygenase-1. *J Clin Invest* 2015; 125: 2609–2625.
10. LeBlanc RH, Chen R, Selim MH, et al. Heme oxygenase-1-mediated neuroprotection in subarachnoid hemorrhage via intracerebroventricular deferoxamine. *J Neuroinflammation* 2016; 13: 244.
11. Kaiser S, Selzner L, Weber J, et al. Carbon monoxide controls microglial erythrophagocytosis by regulating CD36 surface expression to reduce the severity of hemorrhagic injury. *Glia* 2020; 68: 2427–2445.
12. Kaiser S, Frase S, Selzner L, et al. Neuroprotection after hemorrhagic stroke depends on cerebral heme oxygenase-1. *Antioxidants (Basel)* 2019; 8: 496.
13. Goulay R, Flament J, Gauberti M, et al. Subarachnoid hemorrhage severely impairs brain parenchymal cerebrospinal fluid circulation in nonhuman primate. *Stroke* 2017; 48: 2301–2305.
14. Luo C, Yao X, Li J, et al. Paravascular pathways contribute to vasculitis and neuroinflammation after subarachnoid hemorrhage independently of glymphatic control. *Cell Death Dis* 2016; 7: e2160.
15. Macdonald RL and Weir BK. A review of hemoglobin and the pathogenesis of cerebral vasospasm. *Stroke* 1991; 22: 971–982.
16. Sabri M, Jeon H, Ai J, et al. Anterior circulation mouse model of subarachnoid hemorrhage. *Brain Res* 2009; 1295: 179–185.
17. Polfliet MM, Goede PH, van Kesteren-Hendrikx EM, et al. A method for the selective depletion of perivascular and meningeal macrophages in the central nervous system. *J Neuroimmunol* 2001; 116: 188–195.
18. Galea I, Palin K, Newman TA, et al. Mannose receptor expression specifically reveals perivascular macrophages in normal, injured, and diseased mouse brain. *Glia* 2005; 49: 375–384.
19. Yagi K, Lidington D, Wan H, et al. Therapeutically targeting tumor necrosis factor-alpha/sphingosine-1-phosphate signaling corrects myogenic reactivity in subarachnoid hemorrhage. *Stroke* 2015; 46: 2260–2270.
20. Garcia JH, Wagner S, Liu KF, et al. Neurological deficit and extent of neuronal necrosis attributable to middle cerebral artery occlusion in rats. Statistical validation. *Stroke* 1995; 26: 627–635. discussion
21. Shen Z, Lu Z, Chhatbar PY, et al. An artery-specific fluorescent dye for studying neurovascular coupling. *Nat Methods* 2012; 9: 273–276.
22. Faraco G, Park L, Anrather J, et al. Brain perivascular macrophages: characterization and functional roles in health and disease. *J Mol Med (Berl)* 2017; 95: 1143–1152.
23. Bechmann I, Priller J, Kovac A, et al. Immune surveillance of mouse brain perivascular spaces by blood-borne macrophages. *Eur J Neurosci* 2001; 14: 1651–1658.
24. Sofroniew MV and Vinters HV. Astrocytes: biology and pathology. *Acta Neuropathol* 2010; 119: 7–35.
25. Vergouwen MD, Vermeulen M, Coert BA, et al. Microthrombosis after aneurysmal subarachnoid hemorrhage: an additional explanation for delayed cerebral ischemia. *J Cereb Blood Flow Metab* 2008; 28: 1761–1770.
26. McBride DW, Blackburn SL, Peeyush KT, et al. The role of thromboinflammation in delayed cerebral ischemia after subarachnoid hemorrhage. *Front Neurol* 2017; 8: 555.
27. Han SM, Wan H, Kudo G, et al. Molecular alterations in the hippocampus after experimental subarachnoid hemorrhage. *J Cereb Blood Flow Metab* 2014; 34: 108–117.
28. Koide M, Bonev AD, Nelson MT, et al. Inversion of neurovascular coupling by subarachnoid blood depends on large-conductance Ca2+-activated K+ (BK) channels. *Proc Natl Acad Sci U S A* 2012; 109: E1387–95.

29. Goldmann T, Wieghofer P, Jordao MJ, et al. Origin, fate and dynamics of macrophages at central nervous system interfaces. *Nat Immunol* 2016; 17: 797–805.
30. Kierdorf K, Masuda T, Jordao MJC, et al. Macrophages at CNS interfaces: ontogeny and function in health and disease. *Nat Rev Neurosci* 2019; 20: 547–562.
31. Iqbal S, Hayman EG, Hong C, et al. Inducible nitric oxide synthase (NOS-2) in subarachnoid hemorrhage: regulatory mechanisms and therapeutic implications. *Brain Circ* 2016; 2: 8–19.
32. Macdonald RL, Pluta RM and Zhang JH. Cerebral vasospasm after subarachnoid hemorrhage: the emerging revolution. *Nat Clin Pract Neurol* 2007; 3: 256–263.
33. Greenhalgh AD, Rothwell NJ and Allan SM. An endovascular perforation model of subarachnoid haemorrhage in rat produces heterogeneous infarcts that increase with blood load. *Transl Stroke Res* 2012; 3: 164–172.
34. Hawkes CA and McLaurin J. Selective targeting of perivascular macrophages for clearance of beta-amyloid in cerebral amyloid angiopathy. *Proc Natl Acad Sci U S A* 2009; 106: 1261–1266.
35. Park L, Uekawa K, Garcia-Bonilla L, et al. Brain perivascular macrophages initiate the neurovascular dysfunction of Alzheimer abeta peptides. *Circ Res* 2017; 121: 258–269.
36. Klymchenko AS and Kreder R. Fluorescent probes for lipid rafts: from model membranes to living cells. *Chem Biol* 2014; 21: 97–113.
37. Iliff JJ, Wang M, Liao Y, et al. A paravascular pathway facilitates CSF flow through the brain parenchyma and the clearance of interstitial solutes, including amyloid beta. *Sci Transl Med* 2012; 4: 147ra111.
38. Smith AJ, Yao X, Dix JA, et al. Test of the 'glymphatic' hypothesis demonstrates diffusive and aquaporin-4-independent solute transport in rodent brain parenchyma. *Elife* 2017; 6: e27679.
39. DuBoulay GH, Hughes JT, Aitken V, et al. Platelets in the subarachnoid space. A cause of acute and delayed arterial spasm, intimal damage and cerebral infarction. *Acta Neurochir (Wien)* 1987; 89: 64–70.
40. Harada T, Suzuki Y, Satoh S, et al. Blood component induction of cerebral vasospasm. *Neurosurgery* 1990; 27: 252–255; discussion 255-6.
41. Johshita H, Kassell NF and Sasaki T. Blood-brain barrier disturbance following subarachnoid hemorrhage in rabbits. *Stroke* 1990; 21: 1051–1058.